IOP Publishing Physics in Medicine and Biology

Phys. Med. Biol. **52** (2007) 3001–3013 doi:10.1088/0031-9155/52/11/005

Analysis of recoverable current from one component of magnetic flux density in MREIT and MRCDI

Chunjae Park[1], **Byung Il Lee**[2] **and Oh In Kwon**[1]

[1] Department of Mathematics, Konkuk University, Korea
[2] College of Electronics and Information, Kyung Hee University, Korea

E-mail: oikwon@konkuk.ac.kr

Received 20 November 2006, in final form 12 February 2007
Published 4 May 2007
Online at stacks.iop.org/PMB/52/3001

Abstract

Magnetic resonance current density imaging (MRCDI) provides a current density image by measuring the induced magnetic flux density within the subject with a magnetic resonance imaging (MRI) scanner. Magnetic resonance electrical impedance tomography (MREIT) has been focused on extracting some useful information of the current density and conductivity distribution in the subject Ω using measured B_z, one component of the magnetic flux density $\mathbf{B}$. In this paper, we analyze the map $\mathcal{T}$ from current density vector field $\mathbf{J}$ to one component of magnetic flux density B_z without any assumption on the conductivity. The map $\mathcal{T}$ provides an orthogonal decomposition $\mathbf{J} = \mathbf{J}^P + \mathbf{J}^N$ of the current $\mathbf{J}$ where $\mathbf{J}^N$ belongs to the null space of the map $\mathcal{T}$. We explicitly describe the projected current density $\mathbf{J}^P$ from measured B_z. Based on the decomposition, we prove that B_z data due to one injection current guarantee a unique determination of the isotropic conductivity under assumptions that the current is two-dimensional and the conductivity value on the surface is known. For a two-dimensional dominating current case, the projected current density $\mathbf{J}^P$ provides a good approximation of the true current $\mathbf{J}$ without accumulating noise effects. Numerical simulations show that $\mathbf{J}^P$ from measured B_z is quite similar to the target $\mathbf{J}$. Biological tissue phantom experiments compare $\mathbf{J}^P$ with the reconstructed $\mathbf{J}$ via the reconstructed isotropic conductivity using the harmonic B_z algorithm.

1. Introduction

The magnetic resonance current density imaging (MRCDI) technique has been proposed (Eyuboglu *et al* 1999, Gamba *et al* 1999, Joy *et al* 1989, 2004, Scott *et al* 1991, 1992, 1993) by using a magnetic resonance imaging (MRI) scanner. MRCDI measures the internal magnetic flux density $\mathbf{B} = (B_x, B_y, B_z)$ generated by an externally injected electrical current through the electrodes attached to the surface of subject Ω. Ampere law $\mathbf{J} = \nabla \times \mathbf{B}/\mu_0$, where μ_0 is the magnetic permeability of the free space, produces the internal current density

$\mathbf{J} = (J_x, J_y, J_z)$ corresponding to the measured magnetic flux density $\mathbf{B}$. Since an MRI scanner measures only one component of the magnetic flux density $\mathbf{B} = (B_x, B_y, B_z)$ that is parallel to the main magnetic field direction, we have to rotate the subject to measure all three components of $\mathbf{B}$. Indeed, a human body cannot be rotated in a conventional MRI scanner and even if it is possible, the rotation of the subject may cause artifacts by misalignments of pixels and movements of internal organs. To overcome the rotating problem, recently proposed magnetic resonance electrical impedance tomography (MREIT) reconstructs the conductivity and the current density in the subject Ω by measuring only one component B_z data. Instead of rotating a subject, MREIT needs at least two independent current injections to reconstruct the conductivity distribution in Ω.

Most MREIT studies focus on extracting some constructive relations between B_z data and conductivity distributions in the subject Ω (Birgul *et al* 2003, 2006, Gao *et al* 2006, Hamamura *et al* 2006, Ider *et al* 1998, Joy 2004, Kwon *et al* 2002, Lee *et al* 2003, Muftuler *et al* 2004, Park *et al* 2004, Seo *et al* 2004). Although imaging techniques in MREIT using B_z data have been rapidly developed and are at the stage of animal experiments nowadays, we still have lots of theoretical studies in MREIT such as unique determination of the conductivity using B_z data, characteristics of the proposed algorithms, and the relations between the current $\mathbf{J}$ and measured B_z data, etc.

In this paper, we analyze the map $\mathcal{T}$ from current density vector fields $\mathbf{J}$ to one component B_z of magnetic flux density $\mathbf{B}$. We decompose the interior current $\mathbf{J}$ into $\mathbf{J} = \mathbf{J}^P + \mathbf{J}^N$ for $\mathbf{J}^N \in \mathcal{N}(\mathcal{T})$ and $\mathbf{J}^P \in \mathcal{P}(\mathcal{T})$ in which the projected current $\mathbf{J}^P$ does not depend on the conductivity properties. Here, $\mathcal{N}(\mathcal{T})$ and $\mathcal{P}(\mathcal{T})$ are the null space of the map $\mathcal{T}$ and its orthogonal complement space with respect to L^2-scalar product, respectively. After precise descriptions of the map $\mathcal{T}$ and the spaces $\mathcal{N}(\mathcal{T})$ and $\mathcal{P}(\mathcal{T})$, we show that the projected current density $\mathbf{J}^P$ consists of two currents: $\mathbf{J}^{P_1}$ and $\mathbf{J}^{P_2}$. $\mathbf{J}^{P_1}$ is the current corresponding to a homogeneous background conductivity. For $\mathbf{J}^{P_2}$, we construct two-dimensional potential β from measured magnetic flux data B_z.

When the current is two-dimensional, the current $\mathbf{J}$ is uniquely determined from only one B_z data. Based on the decomposition of two-dimensional current, we prove a unique determination of isotropic conductivity using B_z data due to one injection current under the assumption that the conductivity values on the boundary are fixed. We also investigate the meaning of the projected current $\mathbf{J}^P$ of a general three-dimensional current $\mathbf{J}$. For a two-dimensional dominating current case, the projected current density $\mathbf{J}^P$ recovered directly by solving the two-dimensional harmonic equation from measured B_z data provides a good approximation of the true current $\mathbf{J}$ without accumulating noise effects by solving forward problems to update current density and any assumption on the conductivity which is isotropic or anisotropic.

For numerical experiments, we calculate the projected current $\mathbf{J}^P$ from the map $\mathcal{T}$ for a given simulated current $\mathbf{J}$ and magnetic flux data B_z corresponding to anisotropic conductivity $\tilde{\sigma}$. Next, we use measured B_z data with biological tissue phantom experiments using a 3 T MRI scanner. We compare the projected current $\mathbf{J}^P$ and the reconstructed current $\mathbf{J}$ using the harmonic B_z algorithm with two different measured B_z data.

2. Method

2.1. Projected current density $\mathbf{J}^P$ *of* $\mathbf{J}$

Let Ω be a three-dimensional, cylindrical and electrical conducting body with its boundary $\partial\Omega$. This domain can be expressed as the union of slices which are perpendicular to the z-axis:

$$\Omega = \bigcup_{t\in(-H,H)} \Omega_t, \qquad \text{where} \quad \Omega_t = \Omega \cap \{(x, y, z) \in \mathbb{R}^3 \mid z = t\}.$$

Let $\mathbf{n} = (n_1, n_2, n_3)$ be the outward unit normal vector on $\partial\Omega$. We inject current into Ω through a pair of surface electrodes attached to $\partial\Omega$. The interior current density distribution $\mathbf{J} = (J_x, J_y, J_z)$ influenced by the injection current satisfies

$$\begin{aligned} &\nabla \cdot \mathbf{J} = 0 \quad \text{in} \quad \Omega \\ &\mathbf{J} \cdot \mathbf{n} = g \quad \text{on} \quad \partial\Omega. \end{aligned} \tag{1}$$

In a real model, the exterior current $\mathbf{J}^I$ outside of Ω is decided by configurations of lead wires and electrodes attached to $\partial\Omega$. Since we can control the geometry of lead wires and electrodes and the amount of injection current in experimental setups, one can decide the exterior current $\mathbf{J}^I$ outside of Ω and $\mathbf{J} \cdot \mathbf{n}$ on $\partial\Omega$. The total current $\mathbf{J}^T := \mathbf{J} + \mathbf{J}^I$ in whole domain $\mathbb{R}^3$ generates the corresponding magnetic flux density $\mathbf{B}^T := \mathbf{B}^J + \mathbf{B}^I$ where $\mathbf{B}^J$ comes from the internal current density $\mathbf{J}$ in Ω and $\mathbf{B}^I$ is the magnetic flux density generated by the known exterior current $\mathbf{J}^I$. Since $\mathbf{B}^I$ is determined by the known current outside of Ω, we can extract $\mathbf{B}^J$ by measuring $\mathbf{B}^T$. In the remainder of this paper, we simply denote $\mathbf{B}^J$ by $\mathbf{B}$.

Most algorithms developed in MREIT have used the fundamental relation

$$\nabla^2 B_z = \mu_0 \nabla \cdot (-J_y, J_x, 0) = \mu_0 \left(\frac{\partial\sigma}{\partial x}\frac{\partial u}{\partial y} - \frac{\partial\sigma}{\partial y}\frac{\partial u}{\partial x} \right) \tag{2}$$

to obtain distinguishable information of the current $\mathbf{J}$ and the isotropic conductivity σ, where u is the voltage potential corresponding to σ. In this section, we focus on analyzing the relation between the current $\mathbf{J} = (J_x, J_y, J_z)$ and measured data B_z in Ω.

Let $\mathcal{V}$ be a divergence free space as

$$\mathcal{V} := H(\text{div}; \Omega, 0) = \{\mathbf{J} \in H^1(\Omega)^3 \mid \nabla \cdot \mathbf{J} = 0 \text{ in } \Omega\}, \tag{3}$$

where $H^1(\Omega)$ denotes the Sobolev space (Girault *et al* 1986). Define a linear operator $\mathcal{T}$ as

$$\begin{aligned} \mathcal{T} : \quad & \mathcal{V} \longrightarrow L^2(\Omega) \times H^{-\frac{1}{2}}(\partial\Omega) \\ & \mathbf{J} \longmapsto (\nabla^2 B_z, \mathbf{J} \cdot \mathbf{n}). \end{aligned} \tag{4}$$

Biot–Savart law shows the relation between B_z and $\mathbf{J} = (J_x, J_y, J_z)$:

$$B_z(\mathbf{r}) = \frac{\mu_0}{4\pi} \int_\Omega \frac{(y - y')J_x(\mathbf{r}') - (x - x')J_y(\mathbf{r}')}{|\mathbf{r} - \mathbf{r}'|^3}\, d\mathbf{r}'. \tag{5}$$

We decompose the vector space $\mathcal{V}$ into two orthogonal spaces $\mathcal{N}(\mathcal{T})$ and $\mathcal{P}(\mathcal{T})$

$$\mathcal{V} = \mathcal{N}(\mathcal{T}) + \mathcal{P}(\mathcal{T}), \tag{6}$$

where $\mathcal{N}(\mathcal{T})$ is the null space of $\mathcal{T}$ and $\mathcal{P}(\mathcal{T})$ is its orthogonal complement space with respect to the scalar product of $L^2(\Omega)$. The null space of $\mathcal{T}$ is characterized as

$$\mathcal{N}(\mathcal{T}) = \{\mathbf{J} \in \mathcal{V} \mid \nabla^2 B_z = 0 \text{ in } \Omega \text{ and } \mathbf{J} \cdot \mathbf{n} = 0 \text{ on } \partial\Omega\}. \tag{7}$$

For convenience, we denote $\langle \cdot, \cdot \rangle$ a usual $L^2(\Omega)$-inner product and use the notations $\nabla = \left(\frac{\partial}{\partial x}, \frac{\partial}{\partial y}, \frac{\partial}{\partial z}\right)$ and $\tilde{\nabla} = \left(\frac{\partial}{\partial x}, \frac{\partial}{\partial y}\right)$.

We consider that two observable vectors $\mathbf{J}^0 := \nabla\alpha$ and $\mathbf{J}^* := \left(\frac{\partial\beta}{\partial y}, -\frac{\partial\beta}{\partial x}, 0\right)$ belong to $\mathcal{V}$, where α is a homogeneous voltage potential satisfying

$$\begin{aligned} &\nabla^2\alpha = 0 && \text{in} \quad \Omega \\ &\nabla\alpha \cdot \mathbf{n} = \mathbf{J} \cdot \mathbf{n} && \text{on} \quad \partial\Omega \qquad \text{and} \qquad \int_{\partial\Omega} \alpha\, ds = 0 \end{aligned} \tag{8}$$

and $\beta_t(x, y) := \beta(x, y, t)$ satisfies the following two-dimensional Laplace equation for each slice $\Omega_t \subset \Omega$

$$\begin{aligned} \tilde{\nabla}^2 \beta_t &= \tfrac{1}{\mu_0} \nabla^2 B_z \quad \text{in} \quad \Omega_t \\ \beta_t &= 0 \qquad\qquad\quad \text{on} \quad \partial\Omega_t. \end{aligned} \tag{9}$$

For any $\mathbf{J}^N \in \mathcal{N}(\mathcal{T})$, the vector $\mathbf{J}^0 = \nabla\alpha$ from the given injection current density $\mathbf{J} \cdot \mathbf{n}$ on $\partial\Omega$ yields that

$$\begin{aligned} \langle \mathbf{J}^0, \mathbf{J}^N \rangle &= \int_\Omega \mathbf{J}^0(\mathbf{r}) \cdot \mathbf{J}^N(\mathbf{r})\, \mathrm{d}\mathbf{r} \\ &= \int_\Omega \left(\frac{\partial\alpha}{\partial x}, \frac{\partial\alpha}{\partial y}, \frac{\partial\alpha}{\partial z} \right)(\mathbf{r}) \cdot \left(J_x^N, J_y^N, J_z^N \right)(\mathbf{r})\, \mathrm{d}\mathbf{r} \\ &= -\int_\Omega \alpha(\mathbf{r}) \nabla \cdot \mathbf{J}^N(\mathbf{r})\, \mathrm{d}\mathbf{r} + \int_{\partial\Omega} \alpha(\mathbf{r}) \mathbf{J}^N(\mathbf{r}) \cdot \mathbf{n}\, \mathrm{d}s \\ &= 0, \end{aligned} \tag{10}$$

where s is the surface element on $\partial\Omega$. The relation (10) shows that the vector $\mathbf{J}^0$ belongs to $\mathcal{P}(\mathcal{T})$.

Next, the vector $\mathbf{J}^* = \left(\frac{\partial\beta}{\partial y}, -\frac{\partial\beta}{\partial x}, 0 \right)$ satisfies the divergence-free condition and for any $\mathbf{J}^N \in \mathcal{N}(\mathcal{T})$,

$$\begin{aligned} \langle \mathbf{J}^*, \mathbf{J}^N \rangle &= \int_\Omega \mathbf{J}^*(\mathbf{r}) \cdot \mathbf{J}^N(\mathbf{r})\, \mathrm{d}\mathbf{r} \\ &= \int_\Omega \left(\frac{\partial\beta}{\partial y}(\mathbf{r}), -\frac{\partial\beta}{\partial x}(\mathbf{r}), 0 \right) \cdot \left(J_x^N(\mathbf{r}), J_y^N(\mathbf{r}), J_z^N(\mathbf{r}) \right) \mathrm{d}\mathbf{r} \\ &= \int_{-H}^{H} \left(\int_{\Omega_t} \left(\frac{\partial\beta}{\partial x}(\mathbf{r}), \frac{\partial\beta}{\partial y}(\mathbf{r}) \right) \cdot \left(-J_y^N(\mathbf{r}), J_x^N(\mathbf{r}) \right) \mathrm{d}x\, \mathrm{d}y \right) \mathrm{d}t \\ &= -\int_{-H}^{H} \left(\int_{\Omega_t} \beta(\mathbf{r}) \tilde{\nabla} \cdot \left(-J_y^N, J_x^N \right)(\mathbf{r})\, \mathrm{d}x\, \mathrm{d}y \right) \mathrm{d}t \\ &\quad + \int_{-H}^{H} \left(\int_{\partial\Omega_t} \beta(\mathbf{r}) \left(-J_y^N, J_x^N \right)(\mathbf{r}) \cdot \nu\, \mathrm{d}\ell \right) \mathrm{d}t \\ &= 0, \end{aligned} \tag{11}$$

where $\mathrm{d}\ell$ denotes the line element on $\partial\Omega_t$ and $\nu = (\nu_1, \nu_2) = (n_1, n_2)/|(n_1, n_2)|$ is the planar unit normal vector of $\mathbf{n} = (n_1, n_2, n_3)$ projected onto $\partial\Omega_t$. Hence $\mathbf{J}^* \in \mathcal{P}(\mathcal{T})$. According to the calculations in (10) and (11), we can explicitly extract two currents $\mathbf{J}^0$ and $\mathbf{J}^*$ in $\mathcal{P}(\mathcal{T})$ for any current $\mathbf{J}$ in Ω. We now need to answer whether $\mathbf{J}^0$ and $\mathbf{J}^*$ exhaust all projected components of $\mathbf{J}$ or not. To answer the question, set the difference vector $\mathbf{J}^D := \mathbf{J} - \mathbf{J}^0 - \mathbf{J}^*$. It is obvious that $\nabla \cdot \mathbf{J}^D = 0$ because $\nabla \cdot \mathbf{J}^* = \nabla \cdot \left(\frac{\partial\beta}{\partial y}, -\frac{\partial\beta}{\partial x}, 0 \right) = 0$ in Ω. Since β is zero on each $\partial\Omega_t$ in (9), for the Neumann vector $\mathbf{n} = (n_1, n_2, n_3)$ on $\partial\Omega$,

$$\left(\frac{\partial\beta}{\partial y}, -\frac{\partial\beta}{\partial x}, 0 \right) \cdot \mathbf{n} = \tilde{\nabla}\beta \cdot (-n_2, n_1) = \sqrt{n_1^2 + n_2^2}\, \frac{\partial\beta}{\partial\tau} = 0 \qquad \text{on} \quad \partial\Omega, \tag{12}$$

where the vector $\tau = (\tau_1, \tau_2)$ is the unit tangential vector on $\partial\Omega_t$. Thus, we have

$$\mathbf{J}^D \cdot \mathbf{n} = \mathbf{J} \cdot \mathbf{n} - \mathbf{J}^0 \cdot \mathbf{n} - \left(\frac{\partial\beta}{\partial y}, -\frac{\partial\beta}{\partial x}, 0 \right) \cdot \mathbf{n} = 0 \qquad \text{on} \quad \partial\Omega.$$

Moreover, the difference vector $\mathbf{J}^D$ satisfies

$$-\frac{\partial J_y^D}{\partial x} + \frac{\partial J_x^D}{\partial y} = -\frac{\partial J_y}{\partial x} + \frac{\partial J_x}{\partial y} - \tilde{\nabla}^2\beta = \frac{1}{\mu_0}(\nabla^2 B_z - \nabla^2 B_z) = 0 \qquad \text{in} \quad \Omega.$$

This implies that $\mathbf{J}^D \in \mathcal{N}(\mathcal{T})$. Thus, $\mathbf{J}^P = \mathbf{J}^0 + \mathbf{J}^*$ is the unique projection component of $\mathbf{J}$.

2.2. $\mathbf{J}^P$ *for two-dimensional dominant current* $\mathbf{J}$

First, we assume a two-dimensional current $\mathbf{J}(\mathbf{r}) = (J_x(\mathbf{r}), J_y(\mathbf{r}), 0)$ in $\Omega = \cup_{t\in(-H,H)}\Omega_t$. Then, the difference vector $\mathbf{J}^D = \mathbf{J} - \mathbf{J}^P$ of $\mathbf{J}$ on $\mathcal{N}(\mathcal{T})$ satisfies

$$\tilde{\nabla} \times \left(J_x^D(\mathbf{r}), J_y^D(\mathbf{r})\right) = \frac{\partial J_y^D}{\partial x}(\mathbf{r}) - \frac{\partial J_x^D}{\partial y}(\mathbf{r}) = 0 \quad \text{in} \quad \Omega_t \qquad \text{for all} \quad t \in (-H, H). \tag{13}$$

Since the vector $\mathbf{J}^D$ is curl-free in (13), there exists a potential function $h_t(x, y) := h(x, y, t)$ at each Ω_t such that $\mathbf{J}^D = \left(\frac{\partial h}{\partial x}, \frac{\partial h}{\partial y}, 0\right)$. Due to the divergence-free condition of the vector $\mathbf{J}^D$, the scalar function h satisfies

$$\tilde{\nabla}^2 h_t(\mathbf{r}) = 0 \qquad \text{in} \quad \Omega_t \qquad \text{and} \qquad \tilde{\nabla} h_t \cdot \nu = 0 \quad \text{on} \quad \partial\Omega_t, \tag{14}$$

where $\nu = (\nu_1, \nu_2) = (n_1, n_2)/|(n_1, n_2)|$ is the planar unit normal vector of $\mathbf{n}$ projected onto $\partial\Omega_t$. Since a solution of (14) is unique up to constant, we have that $\mathbf{J}^D = \left(\frac{\partial h}{\partial x}, \frac{\partial h}{\partial y}, 0\right) = (0, 0, 0)$ in Ω and $\mathbf{J} = \mathbf{J}^P$, i.e., arbitrary two-dimensional current in Ω can be determined by measuring one B_z.

Infinitely many isotropic conductivity distributions may generate the same current $\mathbf{J}$ in Ω (Kim *et al* 2002, 2003, Kwon *et al* 2002) even when $\mathbf{J}$ is two-dimensional. For these reasons, most developed algorithms for conductivity reconstruction in MREIT use at least two independent injection currents I^i, $i = 1, \ldots, N$ (Birgul *et al* 2003, Gao *et al* 2006, Hamamura *et al* 2006, Ider *et al* 2004, Lee *et al* 2003, 2004, Muftuler *et al* 2004, Park *et al* 2004a, 2004b).

However, from now on we investigate the unique determination of the isotropic conductivity distribution in Ω using one injection current under some conditions. Let us consider the elliptic equation for $0 < \sigma < \infty$:

$$\begin{aligned} &\nabla \cdot \sigma \nabla u = 0 \quad \text{in} \quad \Omega \\ &-\sigma \nabla u \cdot \mathbf{n} = g \quad \text{on} \quad \partial\Omega \qquad \text{and} \qquad \int_{\partial\Omega} u \, \mathrm{d}s = 0. \end{aligned} \tag{15}$$

We assume that the current $\mathbf{J} = -\sigma\nabla u = -\left(\sigma\frac{\partial u}{\partial x}, \sigma\frac{\partial u}{\partial y}, 0\right)$ is two-dimensional and non-vanishing in Ω where the potential u is the solution of (15). If we fix conductivity values on the boundary $\partial\Omega$, then measured B_z using one injection current uniquely determine the interior conductivity σ in Ω.

If we assume that there exist two isotropic conductivities σ and $\tilde{\sigma}$, $\sigma = \tilde{\sigma}$ on $\partial\Omega$, generating the same current $\mathbf{J} = -\sigma\nabla u = -\tilde{\sigma}\nabla v$ in Ω with $\mathbf{J}\cdot\mathbf{n} = g$ on $\partial\Omega$. Here, the potentials u and v are the solution of (15) corresponding to the conductivity σ and $\tilde{\sigma}$, respectively. The conductivity σ and the current $\mathbf{J}$ satisfy the following relation:

$$\tilde{\nabla} \times (J_x, J_y) = -\tilde{\nabla}\sigma \times \tilde{\nabla} u = \frac{\tilde{\nabla}\sigma}{\sigma} \times (J_x, J_y) = \tilde{\nabla} \log\sigma \times (J_x, J_y). \tag{16}$$

Since the conductivity $\tilde{\sigma}$ also satisfies the relation (16), we have

$$\tilde{\nabla} \log\sigma \times (J_x, J_y) = \tilde{\nabla} \log\tilde{\sigma} \times (J_x, J_y). \tag{17}$$

Using the relation (17), two conductivities σ and $\tilde{\sigma}$ satisfy

$$\tilde{\nabla} \log\left(\frac{\sigma}{\tilde{\sigma}}\right) \times (J_x, J_y) = 0 \qquad \text{in} \quad \Omega. \tag{18}$$

Since σ and $\tilde{\sigma}$ have the same value on $\partial\Omega$ by the assumption, there exists a closed curve $\gamma(t), t = [0, 1]$ such that $\log\left(\frac{\sigma}{\tilde{\sigma}}\right)(\gamma(t_1)) = \log\left(\frac{\sigma}{\tilde{\sigma}}\right)(\gamma(t_2))$ for any $t_1, t_2 \in [0, 1]$. Due to the differentiation of $\log\left(\frac{\sigma}{\tilde{\sigma}}\right)$ along the closed curve γ, we get

$$\frac{\mathrm{d}}{\mathrm{d}t}\left(\log\left(\frac{\sigma}{\tilde{\sigma}}\right)(\gamma(t))\right) = \tilde{\nabla} \log\left(\frac{\sigma}{\tilde{\sigma}}\right)(\gamma(t)) \cdot \gamma'(t) = 0. \tag{19}$$

The relation (18) yields that $\tilde{\nabla}\log\left(\frac{\sigma}{\tilde{\sigma}}\right)$ is parallel to the gradient vector $\tilde{\nabla}u$. The potential u is constant on the closed curve γ because

$$\frac{\mathrm{d}u(\gamma(t))}{\mathrm{d}t} = \tilde{\nabla}u(\gamma(t)) \cdot \gamma'(t) = 0.$$

Thus, there exists a critical point $\mathbf{r}_0 = (x_0, y_0, z_0)$ such that $\tilde{\nabla}u(\mathbf{r}_0) = (0, 0)$ in the interior region of the closed curve $\gamma(t)$. The existence of such a critical point $\mathbf{r}_0$ contradicts the assumption that $\mathbf{J}$ is non-vanishing. Consequently, we have $\sigma = \tilde{\sigma}$.

We consider the projected current $\mathbf{J}^P$ for a more general current $\mathbf{J}$. For a general three-dimensional current $\mathbf{J}$, the projected current $\mathbf{J}^P$ is not equal to the current $\mathbf{J}$. The difference vector $\mathbf{J}^D = \mathbf{J} - \mathbf{J}^P$ may not be determined by measured data $(\nabla^2 B_z, \mathbf{J}\cdot\mathbf{n})$. However, it can be estimated by the differences $J_z - J_z^0$ and $\frac{\partial J_z}{\partial z} - \frac{\partial J_z^0}{\partial z}$ where $\mathbf{J}^0$ is the current corresponding to the homogeneous background material.

Assume that the current injected transversally in a cylindrical domain $\Omega = \cup_{t\in(-H,H)}\Omega_t$ so that $\mathbf{J}\cdot(0, 0, 1) = 0$ on $\partial\Omega$. We consider the potential $f_t(x, y) = f(x, y, t)$ for each slice Ω_t

$$\begin{aligned} &\tilde{\nabla}^2 f_t = \frac{\partial\left(J_z^0 - J_z\right)}{\partial z} && \text{in} \quad \Omega_t \\ &\tilde{\nabla} f_t \cdot \nu = 0 && \text{on} \quad \partial\Omega_t \qquad \text{and} \qquad \int_{\partial\Omega_t} f_t \,\mathrm{d}\ell = 0. \end{aligned} \tag{20}$$

By setting $\tilde{\mathbf{J}} := \mathbf{J} - \left(\frac{\partial f}{\partial x}, \frac{\partial f}{\partial y}, J_z - J_z^0\right) - \mathbf{J}^0$, the vector $\tilde{\mathbf{J}} = \left(J_x - J_x^0 - \frac{\partial f}{\partial x}, J_y - J_y^0 - \frac{\partial f}{\partial y}, 0\right)$ is a two-dimensional current with the known boundary condition on $\partial\Omega_t$:

$$\tilde{\mathbf{J}}\cdot\mathbf{n} = J_x n_1 + J_y n_2 - J_x^0 n_1 - J_y^0 n_2 - \frac{\partial f}{\partial x} n_1 - \frac{\partial f}{\partial y} n_2 = 0.$$

Simple calculations show that $\mathcal{T}(\mathbf{J} - \mathbf{J}^0) = \mathcal{T}(\tilde{\mathbf{J}})$ by (2). Since the current $\tilde{\mathbf{J}}$ is a two-dimensional current, the projected current $\tilde{\mathbf{J}}^P$ coincides with the current $\tilde{\mathbf{J}}$ and also $\tilde{\mathbf{J}}^P = (\mathbf{J} - \mathbf{J}^0)^P = \mathbf{J}^P - \mathbf{J}^0$. Therefore we have

$$\begin{aligned} \|\mathbf{J} - \mathbf{J}^P\| &= \|(\mathbf{J} - \mathbf{J}^0) - (\mathbf{J} - \mathbf{J}^0)^P\| \\ &= \left\|\tilde{\mathbf{J}} + \left(\frac{\partial f}{\partial x}, \frac{\partial f}{\partial y}, J_z - J_z^0\right) - \tilde{\mathbf{J}}^P\right\| \\ &= \left\|\left(\frac{\partial f}{\partial x}, \frac{\partial f}{\partial y}, J_z - J_z^0\right)\right\| \\ &\leqslant \|\tilde{\nabla} f\| + \left\|J_z - J_z^0\right\|, \end{aligned}$$

where $\|\cdot\|$ denotes a usual L^2-norm in Ω. If $\left\|J_z - J_z^0\right\|$ and $\left\|\frac{\partial J_z}{\partial z} - \frac{\partial J_z^0}{\partial z}\right\|$ are smaller than a positive value ϵ, then $\|\tilde{\nabla} f\| \leqslant C\epsilon$ by a standard elliptic theory where the constant C does not depend on $\mathbf{J}$.

3. Results

3.1. Simulation study

In this section, we carry out numerical simulations to extract the projected current $\mathbf{J}^P$ for a given current $\mathbf{J}$ and the magnetic flux B_z induced by $\mathbf{J}$. We consider a general three-dimensional current $\mathbf{J}$, in which the conductivity is anisotropic with considerable differences in distribution. Let $\Omega = [0, 1]^3$ be a cubic domain and set a Neumann flux g such that

$$g(x, y, z) = \begin{cases} 1, & \text{if} \quad \left|x - \frac{1}{4}\right| \leqslant \frac{1}{16}, y = 0, \quad \text{and} \quad \left|z - \frac{3}{8}\right| \leqslant \frac{1}{16} \\ -1, & \text{if} \quad \left|x - \frac{3}{4}\right| \leqslant \frac{1}{16}, y = 1, \quad \text{and} \quad \left|z - \frac{5}{8}\right| \leqslant \frac{1}{16} \\ 0, & \text{otherwise.} \end{cases}$$

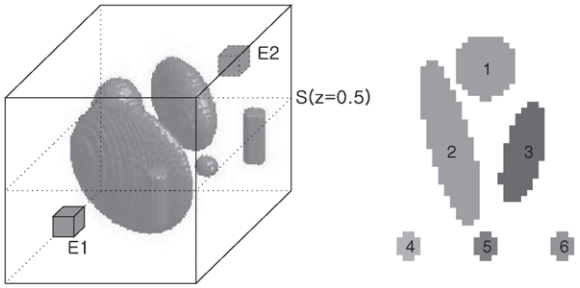

(a) (b)

Figure 1. Anisotropic conductivity distribution with six anomalies. (a) Conductivity distribution in Ω. (b) Cross-sectional image on S.

Table 1. Anisotropic conductivity values at each organ.

Target	σ_{11}	σ_{22}	σ_{33}	σ_{12}	σ_{13}	σ_{23}	λ_M	λ_m
1	0.333	0.991	1.876	0.224	−0.378	−0.141	2.000	0.200
2	4.960	3.078	5.962	0.390	0.188	0.037	6.000	3.000
3	0.124	0.292	0.284	0.037	−0.053	0.011	0.300	0.100
4	6.000	3.000	7.000	0.000	0.000	0.000	7.000	3.000
5	4.938	7.247	4.815	0.782	0.107	−1.354	8.000	4.000
6	0.227	0.299	0.374	−0.028	0.061	−0.011	0.400	0.200

This Neumann condition g is the outward normal component of the current on $\partial\Omega$ where the electrodes $E1$ and $E2$ are attached as in figure 1(a). To generate a target current, we use an anisotropic conductivity distribution $\tilde{\sigma}$ composed of six separate organs with the background conductivity value $\sigma_0 = 1$ in figure 1. The location and shape of each organ are presented in figure 1(a) and the cross-sectional image of $\tilde{\sigma}$ on $z = 0.5$ plane is shown in figure 1(b). Table 1 shows that conductivity values of each anomaly, $\tilde{\sigma} = (\sigma_{ij})$, $i, j = 1, \ldots, 3$, $(i \leqslant j)$. λ_M and λ_m are the largest and smallest eigenvalues of each anomaly, respectively.

Then the target current $\mathbf{J}$ is given by $\mathbf{J} = -\tilde{\sigma}\nabla u$ where u is the solution of

$$\nabla \cdot (\tilde{\sigma}\nabla u) = 0 \quad \text{in} \quad \Omega - \tilde{\sigma}\nabla u \cdot \mathbf{n} = g \quad \text{on} \quad \partial\Omega.$$

The projected current $\mathbf{J}^P$ is given by $\mathbf{J}^P = \mathbf{J}^0 + \left(-\frac{\partial\beta}{\partial y}, \frac{\partial\beta}{\partial x}, 0\right)$ where the current $\mathbf{J}^0 = \nabla\alpha$, the function α is the solution of equation (8) corresponding to the homogeneous background conductivity $\sigma_0 = 1$ and β is the spacial potential which is obtained on each slice Ω_t by solving (9). Note that the background current $\mathbf{J}^0$ does not give any information of the conductivity in Ω. We depict the currents $\delta\mathbf{J} = \mathbf{J} - \mathbf{J}^0$ and $\delta\mathbf{J}^P = \mathbf{J}^P - \mathbf{J}^0 = \left(-\frac{\partial\beta}{\partial y}, \frac{\partial\beta}{\partial x}, 0\right)$ at the $z = 0.5$ plane in figure 2. Although there is no zth current component in $\delta\mathbf{J}^P$, the intensity image of $\delta\mathbf{J}^P$ has considerable information of the true image of $|\delta\mathbf{J}|$ as in the right column of figure 2.

In section 2.2, we show that the difference current $\mathbf{J} - \mathbf{J}^P$ only depends on the zth component $J_z - J_z^0$. Since the difference $J_z - J_z^0$ relates to $\tilde{\sigma} - \sigma_0$, for the given conductivity distribution $\tilde{\sigma}$ in table 1, we can define $\sigma_c := c(\tilde{\sigma} - \sigma_0) + \sigma_0$.

For several $c = 0.2, 0.4, 0.6, 0.8$ and 1, the relative errors $E_a (a = x, y, z)$ between the projected current $\mathbf{J}^P$ and $\mathbf{J}$ defined by

$$E_a := \frac{\left\| J_a - J_a^P \right\|}{\| J_a \|} \tag{21}$$

are shown in table 2.

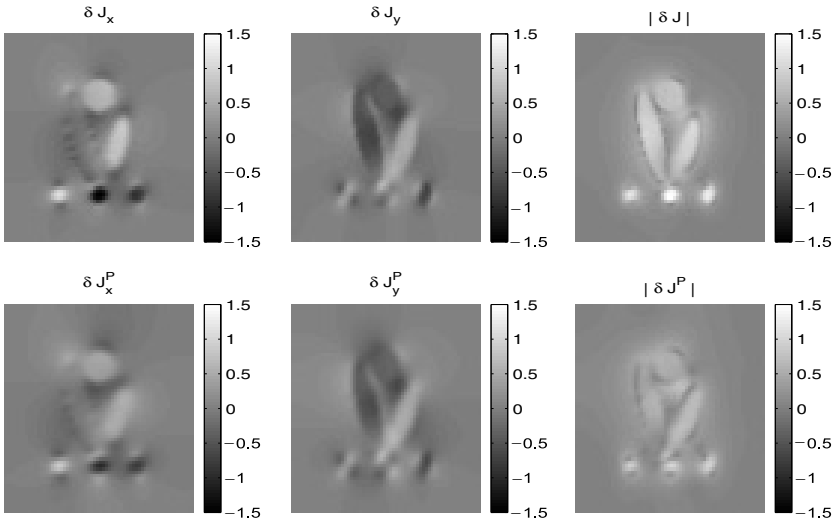

Figure 2. Simulation experiment: difference current images of $\delta\mathbf{J}$ and $\delta\mathbf{J}^P$ are depicted in the left and center columns, respectively. The right column is the images of $|\delta\mathbf{J}|$ and $|\delta\mathbf{J}^P|$.

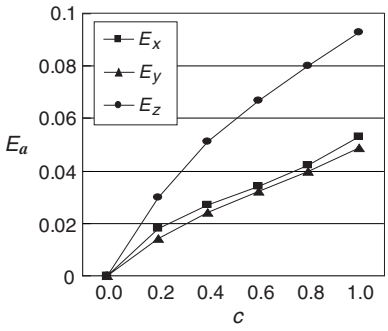

Figure 3. Relative error plot for $c = 0.2, 0.4, \ldots, 1$.

Table 2. Relative errors E_a for various $c = 0.2, 0.4, \ldots, 1$.

c	E_x	E_y	E_z
0.2	0.018	0.014	0.030
0.4	0.027	0.024	0.051
0.6	0.034	0.032	0.067
0.8	0.042	0.040	0.080
1	0.053	0.049	0.093

3.2. Biological tissue phantom experiment

We compute the projected current $\mathbf{J}^P$ using real experimental MREIT data. The magnetic flux B_z data using a 3 T MRI scanner are measured for a three-dimensional phantom containing different biological tissues embedded in agar-gel; bovine tongue, porcine muscle and chicken

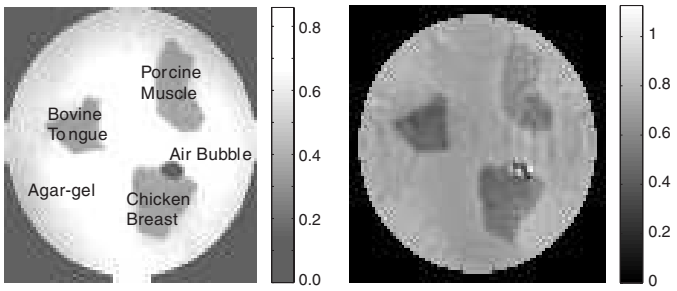

Figure 4. (a) MR magnitude image of the biological tissue phantom. (b) Reconstructed conductivity image using the harmonic B_z algorithm.

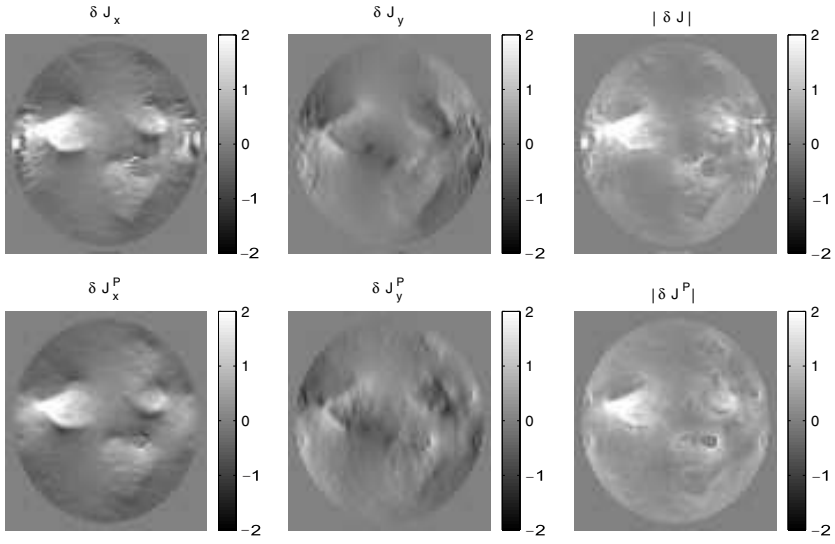

Figure 5. Biological tissue phantom experiment: difference current images of $\delta\mathbf{J}$ and $\delta\mathbf{J}^P$ are represented in the left and center columns, respectively. The right column is the images of $|\delta\mathbf{J}|$ and $|\delta\mathbf{J}^P|$.

breast. The phantom has a cylindrical shape with a diameter and height of 140 mm. We attached four electrodes with equal spacing among them and the size of each recessed electrode was 10×20 mm^2. More details on the experimental setup are given in Oh *et al* (2005). We input current with strength 48 mA. Figure 4(a) shows its magnitude image on the center slice of the phantom.

In this paper, we used the harmonic B_z algorithm (Oh *et al* 2003) to reconstruct the isotropic conductivity image of the center slice in figure 4(b). In fact, we do not know that the electrical properties of the biological tissues, bovine tongue, porcine muscle and chicken breast, are isotropic. However, in order to compare the projected current density proposed in this paper and the current density through the reconstructed conductivity, we assume the biological tissues are isotopic. Under the isotropic assumption, the mean reconstructed conductivity values are 0.53, 0.44, 0.59 and 0.73 S m^{-1} for chicken breast, bovine tongue,

porcine muscle and agar gelation, respectively. Here, two independent currents are injected transversally through the four attached electrodes for the harmonic B_z algorithm. We constrain the conductivity value of the air bubble area in figure 4(a) to be zero in the reconstruction since MR signals could not be obtained in that area.

The upper row of figure 5 represents δJ_x, δJ_y and $|\delta \mathbf{J}|$ and the lower row of figure 5 shows δJ_x^P, δJ_y^P and $|\delta \mathbf{J}^P|$. Note that the current $\mathbf{J} = -\sigma \nabla u$ in the upper row of figure 5 is recovered by solving the elliptic equation (15) with the reconstructed isotropic conductivity σ using the iterative harmonic B_z algorithm which needs at least two injection currents. To obtain the current $\mathbf{J}^P$ in the lower row of figure 5, we only need to solve the two-dimensional Laplace equation (9) on the center slice of Ω using measured B_z data induced by one injection current.

The relative errors $E_a(a = x, y, z)$ between the projected current $\mathbf{J}^P$ and $\mathbf{J}$ in figure 5 are 0.026, 0.039 and 0.074 for E_x, E_y and E_z, respectively. Since we attached the electrodes at the middle of the phantom, the internal current by injected current is transversal-dominant. The values of $E_a(a = x, y, z)$ in this phantom experiment show that the projected current $\mathbf{J}^P$ is feasible in real experiments when the internal current is transversal-dominant.

One notable thing is that the reconstructed current $\mathbf{J} = -\sigma \nabla u$ in the upper row of figure 5 needs conductivity reconstructed in advance with B_z for at least two independent injection currents. It may provide a more defective image near the electrode than $\mathbf{J}^P$ in the lower row of figure 5 because it is hard to avoid noise amplification of the reconstructed conductivity near the electrode and in the region where the interior current flows are almost parallel for all injected currents.

4. Discussion

In this paper, we investigate the projected current $\mathbf{J}^P$, which is an optimal detectable current from measured magnetic flux density B_z influenced by one injected current. The projected current $\mathbf{J}^P$ consists of the background current $\mathbf{J}^0$ and the two-dimensional current $\mathbf{J}^*$ by solving the two-dimensional harmonic forward problem (9). Since the background current $\mathbf{J}^0$ which is a homogenous harmonic solution by solving (8) does not contain any information of interior inhomogeneous conductivity, most information of current influenced by inhomogeneous anomaly is in $\mathbf{J}^*$ which is displayed in figures 2 and 5. Moreover, $\mathbf{J}^*$ can be reconstructed immediately by solving the two-dimensional harmonic equation in the region of interest without any assumption on the conductivity.

The real phantom experiment shows that reconstructed $\mathbf{J}^P$ (the lower row in figure 5) is considerably similar to the current via conductivity reconstruction (the upper row in figure 5), in which to reconstruct conductivity we updated conductivity three times and solved three-dimensional forward problems at each update step. The current $\delta \mathbf{J}$ through the reconstructed conductivity using the harmonic B_z algorithm in figure 5 (upper row) depends on the reconstruction algorithm. Thus, the images in the upper row of figure 5 may be changed by using other reconstruction algorithms (Muftuler *et al* 2004, Park *et al* 2004a, 2004b). The reconstructed conductivity using the harmonic B_z algorithm needs the boundary conductivity value which can be determined theoretically by solving the boundary integral equation (Oh *et al* 2003). In this paper, we directly use the background agar value as the boundary conductivity value to reduce noise effects because the boundary value of the measured magnetic flux density is noisy. The harmonic B_z algorithm to reconstruct isotropic conductivity distribution using two injection currents can determine the boundary conductivity by solving the boundary integral equation, but for real-life experiments it is problematic to obtain a good quality of the conductivity near the boundary.

We obtained the projected current $\mathbf{J}^P$ without any assumptions on the conductivity. However, restricting the space $\mathcal{V}$ in (3) to the set $\tilde{\mathcal{V}} := \{\mathbf{J} \in \mathcal{V} \mid \mathbf{J} = -\sigma\nabla u\}$ where σ is the isotropic conductivity, we expect that the projected current $\tilde{\mathbf{J}}^P$ in $\tilde{\mathcal{V}}$ of the current $\mathbf{J}$ is closer to $\mathbf{J}$ than $\mathbf{J}^P$ in $\mathcal{V}$. Theoretically, we proved a unique determination of isotropic conductivity with B_z data due to one injection current when the current is two-dimensional and the isotropic conductivity value is fixed on the boundary $\partial\Omega$. Despite the uniqueness of conductivity under the assumptions, it is difficult to develop an efficient algorithm to reconstruct the interior conductivity distribution using one injection current and one measured magnetic flux density. As far as the authors know, there is no efficient algorithm to reconstruct the conductivity with one injection current because the determination of the conductivity distribution heavily depends on the current pathway; large changes in conductivity may cause very small changes in current in some regions. These are the main reasons that various algorithms developed to recover the conductivity distribution assume the interior property $\mathbf{J}^i \times \mathbf{J}^j \neq 0$ in Ω if $i \neq j$, where the currents $\mathbf{J}^k, k = 1, \ldots, N$ correspond to different independent injection currents. Developing a new algorithm to reconstruct the conductivity distribution using the proposed projected current $\mathbf{J}^P$ will be valuable work. Our future work will include analysis of the relation between $\mathbf{J}^P$ and the conductivity and development of an efficient reconstruction algorithm for conductivity.

5. Conclusions

We rigorously analyze the map $\mathcal{T}$ from currents $\mathbf{J}$ to one component B_z of the magnetic flux density $\mathbf{B}$ and decompose the current $\mathbf{J}$ into $\mathbf{J} = \mathbf{J}^P + \mathbf{J}^N$ where the current $\mathbf{J}^P$ is recovered from measured B_z data. The projected current $\mathbf{J}^P$ is orthogonal to $\mathbf{J}^N$ which belongs to the null space of the map $\mathcal{T}$. The current $\mathbf{J}^P$ is explicitly described as $\mathbf{J}^P = \mathbf{J}^0 + \left(\frac{\partial\beta}{\partial y}, -\frac{\partial\beta}{\partial x}, 0\right)$ where $\mathbf{J}^0$ is the current corresponding to the homogeneous conductivity and the potential β comes from measured B_z data. We show that the difference of $\mathbf{J}$ and $\mathbf{J}^P$ only depends on the zth component $J_z - J_z^0$. Especially, when the current $\mathbf{J}$ is two-dimensional, the projected current $\mathbf{J}^P$ is equal to $\mathbf{J}$ and $\mathbf{J}^P$ uniquely determine an isotropic conductivity if the conductivity value is fixed on the boundary. We reconstruct the projected current $\mathbf{J}^P$ in a stable manner from real experimental MREIT data and compare it with the recovered $\tilde{\mathbf{J}}$ using the harmonic B_z algorithm.

Acknowledgments

Oh In Kwon was supported by the Korea Research Foundation Grant funded by the Korean Government (MOEHRD) (KRF-2005-201-C00004). This work was supported by the SRC/ERC program of MOST/KOSEF (R11-2002-103).

References

Alessandrini G, Isakow V and Powell J 1995 Local uniqueness in the inverse problem with one measurement *Trans. Am. Math. Soc.* **347** 3031–41

Alessandrini G and Magnanini R 1992 The index of isolated critical points and solutions of elliptic equations in the plane *Ann. Scuola Norm. Sup. Pisa Cl. Sci.* **19** 567–89

Birgul O, Eyuboglu B M and Ider Y Z 2003 Current constrained voltage scaled reconstruction (CCVSR) algorithm for MR-EIT and its performance with different probing current patterns *Phys. Med. Biol.* **48** 653–71

Birgul O, Hamamura M J, Muftuler L T and Nalcioglu O 2006 Contrast and spatial resolution in MREIT using low amplitude current *Phys. Med. Biol.* **51** 5035–50

Eyuboglu M, Birgul O and Ider Y Z 2001 A dual modality system for high resolution: true conductivity imaging *Proc. 11th Int. Conf. on Electrical Bioimpedance (ICEBI)* pp 409–13

Eyuboglu M, Reddy R and Leigh J S 1999 Imaging electrical current density using nuclear magnetic resonance *Elektrik* **6** 201–14

Gamba H R, Bayford D and Holder D 1999 Measurement of electrical current density distribution in a simple head phantom with magnetic resonance imaging *Phys. Med. Biol.* **44** 281–91

Gao N, Zhu S A and He B A 2006 New magnetic resonance electrical impedance tomography (MREIT) algorithm: the RSM-MREIT algorithm with applications to estimation of human head conductivity *Phys. Med. Biol.* **51** 3067–83

Ghiglia D C and Pritt M D 1998 *Two-Dimensional Phase Unwrapping: Theory, Algorithms and Software* (New York: Wiley Interscience)

Girault V and Raviart P A 1986 *Finite Element Methods for the Navier Stokes Equations* (SCM 5) (Berlin: Springer)

Hamamura M J, Muftuler L T, Birgul O and Nalcioglu O 2006 Measurement of ion diffusion using magnetic resonance electrical impedance tomography *Phys. Med. Biol.* **51** 2753–62

Holder D (ed) 2005 *Electrical Impedance Tomography: Methods, History and Applications* (Bristol: IOP)

Ider Y Z and Birgul O 1998 Use of the magnetic field generated by the internal distribution of injected currents for electrical impedance tomography (MR-EIT) *Elektrik* **6** 215–25

Ider Y Z and Onart S 2004 Algebraic reconstruction for 3D MR-EIT using one component of magnetic flux density *Physiol. Meas.* **25** 281–94

Joy M L 2004 MR current density and conductivity imaging: the state of the art *Proc. 26th Ann. Int. Conf. IEEE EMBS (San Francisco, CA)* pp 5315–9

Joy M L G, Scott G C and Henkelman R M 1989 In vivo detection of applied electric currents by magnetic resonance imaging *Magn. Reson. Imaging* **7** 89–94

Khang H S, Lee B I, Oh S H, Woo E J, Lee S Y, Cho M H, Kwon O, Yoon J R and Seo J K 2002 *J*-substitution algorithm in magnetic resonance electrical impedance tomography (MREIT): phantom experiments for static resistivity images *IEEE Trans. Med. Imaging* **21** 695–702

Kim S W, Kwon O, Seo J K and Yoon J R 2002 On a nonlinear partial differential equation arising in magnetic resonance electrical impedance tomography *SIAM J. Math. Anal.* **34** 511–26

Kim Y J, Kwon O, Seo J K and Woo E J 2003 Uniqueness and convergence of conductivity image reconstruction in magnetic resonance electrical impedance tomography *Inverse Problems* **19** 1213–25

Kwon O, Woo E J, Yoon J R and Seo J K 2002 Magnetic resonance electrical impedance tomography (MREIT): simulation study of J-substitution algorithm *IEEE Trans. Biomed. Eng.* **48** 160–7

Lee B I, Oh S H, Woo E J, Lee S Y, Cho M H, Kwon O, Seo J K, Lee J Y and Baek W S 2003 Three-dimensional forward solver and its performance analysis in magnetic resonance electrical impedance tomography (MREIT) using recessed electrodes *Phys. Med. Biol.* **48** 1971–86

Lee B I, Lee S H, Kim T S, Kwon O, Woo E J and Seo J K 2005 Harmonic decomposition in PDE-based denoising technique for magnetic resonance electrical impedance tomography *IEEE Trans. Biomed. Eng.* **52** 1912–20

Lee J Y 2004 A reconstruction formula and uniqueness of conductivity in MREIT using two internal current distributions *Inverse Problems* **20** 847–58

Muftuler L, Hamamura M, Birgul O and Nalcioglu O 2004 Resolution and contrast in magnetic resonance electrical impedance tomography (MREIT) and its application to cancer imaging *Technol. Cancer Res. Treatment* **3** 599–609

Oh S H, Lee B I, Park T S, Lee S Y, Woo E J, Cho M H, Kwon O and Seo J K 2004 Magnetic resonance electrical impedance tomography at 3 Tesla field strength *Mag. Reson. Med.* **51** 1292–6

Oh S H, Lee B I, Woo E J, Lee S Y, Cho M H, Kwon O and Seo J K 2003 Conductivity and current density image reconstruction using harmonic B_z algorithm in magnetic resonance electrical impedance tomography *Phys. Med. Biol.* **48** 3101–16

Oh S H, Lee B I, Woo E J, Lee S Y, Kim T S, Kwon O and Seo J K 2005 Electrical conductivity images of biological tissue phantoms in MREIT *Physiol. Meas.* **26** S279–88

Park C, Kwon O, Woo E J and Seo J K 2004b Electrical conductivity imaging using gradient B_z decomposition algorithm in magnetic resonance electrical impedance tomography (MREIT) *IEEE Trans. Med. Imaging* **23** 388–94

Park C, Park E J, Woo E J, Kwon O and Seo J K 2004a Static conductivity imaging using variational gradient B_z algorithm in magnetic resonance electrical impedance tomography *Physiol. Meas.* **25** 257–69

Pyo H C, Kwon O, Seo J K and Woo E J 2005 Identification of current density distribution in electrically conducting subject with anisotropic conductivity distribution *Phys. Med. Biol.* **50** 3183–96

Sadleir R *et al* 2005 Noise analysis in MREIT at 3 and 11 T field strength *Physiol. Meas.* **26** 875–84

Scott G C 1993 NMR imaging of current density and magnetic fields *PhD Thesis* Department of Elec. Eng., University of Toronto, Toronto, Canada

Scott G C, Joy M L G, Armstrong R L and Henkelman R M 1991 Measurement of nonuniform current density by magnetic resonance *IEEE Trans. Med. Imaging* **10** 362–74

Scott G C, Joy M L G, Armstrong R L and Hankelman R M 1992 Sensitivity of magnetic resonance current density imaging *J. Magn. Reson.* **97** 235–54

Seo J K, Kwon O, Lee B I and Woo E J 2003a Reconstruction of current density distributions in axially symmetric cylindrical sections using one component of magnetic flux density: computer simulation study *Physiol. Meas.* **24** 565–77

Seo J K, Pyo H C, Park C J, Kwon O and Woo E J 2004 Image reconstruction of anisotropic conductivity tensor distribution in MREIT: computer simulation study *Phys. Med. Biol.* **49** 4371–82

Seo J K, Yoon J R, Woo E J and Kwon O 2003b Reconstruction of conductivity and current density images using only one component of magnetic field measurements *IEEE Trans. Biomed. Eng.* **50** 1121–4

Woo E J, Lee S Y and Mun C W 1994 Impedance tomography using internal current density distribution measured by nuclear magnetic resonance *Proc. SPIE* **2299** 377–85

Woo E J, Seo J K and Lee S Y 2005 Magnetic resonance electrical impedance tomography (MREIT) *Electrical Impedance Tomography: Methods, History and Applications* ed D Holder (Bristol: IOP)

Zhang N 1992 Electrical impedance tomography based on current density imaging *MS Thesis* Department of Elec. Eng., University of Toronto, Toronto, Canada